NASA/TM—2017-219523

Additive Manufacturing of NiTiHf High Temperature Shape Memory Alloy

Othmane Benafan and Glen S. Bigelow
Glenn Research Center, Cleveland, Ohio

Mohammad Elahinia, Narges Shayesteh Moghaddam, and Amirhesam Amerinatanzi
University of Toledo, Toldeo, Ohio

Soheil Saedi, Guher Pelin Toker, and Haluk Karaca
University of Kentucky, Lexington, Kentucky

June 2017

NASA STI Program . . . in Profile

Since its founding, NASA has been dedicated to the advancement of aeronautics and space science. The NASA Scientific and Technical Information (STI) Program plays a key part in helping NASA maintain this important role.

The NASA STI Program operates under the auspices of the Agency Chief Information Officer. It collects, organizes, provides for archiving, and disseminates NASA's STI. The NASA STI Program provides access to the NASA Technical Report Server—Registered (NTRS Reg) and NASA Technical Report Server—Public (NTRS) thus providing one of the largest collections of aeronautical and space science STI in the world. Results are published in both non-NASA channels and by NASA in the NASA STI Report Series, which includes the following report types:

- TECHNICAL PUBLICATION. Reports of completed research or a major significant phase of research that present the results of NASA programs and include extensive data or theoretical analysis. Includes compilations of significant scientific and technical data and information deemed to be of continuing reference value. NASA counter-part of peer-reviewed formal professional papers, but has less stringent limitations on manuscript length and extent of graphic presentations.

- TECHNICAL MEMORANDUM. Scientific and technical findings that are preliminary or of specialized interest, e.g., "quick-release" reports, working papers, and bibliographies that contain minimal annotation. Does not contain extensive analysis.

- CONTRACTOR REPORT. Scientific and technical findings by NASA-sponsored contractors and grantees.

- CONFERENCE PUBLICATION. Collected papers from scientific and technical conferences, symposia, seminars, or other meetings sponsored or co-sponsored by NASA.

- SPECIAL PUBLICATION. Scientific, technical, or historical information from NASA programs, projects, and missions, often concerned with subjects having substantial public interest.

- TECHNICAL TRANSLATION. English-language translations of foreign scientific and technical material pertinent to NASA's mission.

For more information about the NASA STI program, see the following:

- Access the NASA STI program home page at http://www.sti.nasa.gov

- E-mail your question to help@sti.nasa.gov

- Fax your question to the NASA STI Information Desk at 757-864-6500

- Telephone the NASA STI Information Desk at 757-864-9658

- Write to:
  NASA STI Program
  Mail Stop 148
  NASA Langley Research Center
  Hampton, VA 23681-2199

NASA/TM—2017-219523

Additive Manufacturing of NiTiHf High Temperature Shape Memory Alloy

Othmane Benafan and Glen S. Bigelow
Glenn Research Center, Cleveland, Ohio

Mohammad Elahinia, Narges Shayesteh Moghaddam, and Amirhesam Amerinatanzi
University of Toledo, Toldeo, Ohio

Soheil Saedi, Guher Pelin Toker, and Haluk Karaca
University of Kentucky, Lexington, Kentucky

National Aeronautics and
Space Administration

Glenn Research Center
Cleveland, Ohio 44135

June 2017

Acknowledgments

Funding support from the NASA Glenn Research Center, Transformational Tools & Technologies (TTT) Project is gratefully acknowledged. Specimen additive manufacturing was conducted at University of Toledo under contract #NNC16VA75P.

This work was sponsored by the
Transformative Aeronautics Concepts Program.

Level of Review: This material has been technically reviewed by technical management.

Available from

NASA STI Program
Mail Stop 148
NASA Langley Research Center
Hampton, VA 23681-2199

National Technical Information Service
5285 Port Royal Road
Springfield, VA 22161
703-605-6000

This report is available in electronic form at http://www.sti.nasa.gov/ and http://ntrs.nasa.gov/

Additive Manufacturing of NiTiHf High Temperature Shape Memory Alloy

Othmane Benafan and Glen S. Bigelow
National Aeronautics and Space Administration
Glenn Research Center
Cleveland, Ohio 44135

Mohammad Elahinia, Narges Shayesteh Moghaddam, and Amirhesam Amerinatanzi
University of Toledo
Toldeo, Ohio 43606

Soheil Saedi, Guher Pelin Toker, and Haluk Karaca
University of Kentucky
Lexington, Kentucky 40506

Summary

A NiTi-20Hf high temperature shape memory alloy (HTSMA) was additively manufactured and its shape memory properties were characterized. A selective laser melting (SLM) process was used to fabricate components from NiTiHf powder (of approximately 25 to 75 μm particle fractions), and the thermomechanical response was compared to the conventionally vacuum induction skull melted counterpart. Transformation temperatures of the SLM material were found to be above 200 °C and slightly lower due to the additional O gain from the gas atomization and melting process. The shape memory response in compression was measured for stresses up to 500 MPa, and transformation strains were found to be comparable (up to 1.26 percent for the as-extruded; up to 1.52 percent for SLM).

Nomenclature

A_f	austenite finish
AM	additive manufacturing
A_s	austenite start
CAD	computer-aided design
CBIM	copper boat induction melting
CCLM	cold crucible levitation melting
DSC	differential scanning calorimetry
EBM	electron beam melting
EIGA	electrode induction-melting gas atomization
HTSMA	high temperature shape memory alloy
ICP–AES	inductively coupled plasma atomic emission spectroscopy
LED	light-emitting diode
M_f	martensite finish
M_s	martensite start
PAM	plasma arc melting
SEM	scanning electron microscope
SMA	shape memory alloy
SLM	selective laser melting

TT	transformation temperature
TTT	Transformational Tools & Technologies
TWSME	two-way shape-memory effect
VAM	vacuum arc melting
VIM	vacuum induction melting

Introduction

Commercially available NiTi shape memory alloys (SMAs) present transformation temperatures (TTs) below 100 °C, enabling their practical applications for the many technological applications requiring low operating temperatures, such as biomedical implants and actuators (Refs. 1 to 3). In recent years, NiTi-based high temperature shape memory alloys (HTSMAs) have been introduced via substitution of Ni or Ti by a third element such as Hf, Zr, Pt, Pd, or Au (Refs. 4 to 11). NiTi-based HTSMAs are designed to operate at temperatures above 100 °C, which particularly enable their applications in aerospace, automotive, oil, and many other industries. Among the ternary elements, Hf has attracted much attention due to its high influence on the TT as well as its relatively low cost (Refs. 11 to 13).

It is well documented that the TT of NiTiHf is highly dependent on its composition (Refs. 14 and 15). Nonetheless, up to 10 at.% Hf does not have much influence on the TT, while Hf concentrations higher than 10 at.% linearly increase the TT of (Ti+Hf)-rich NiTiHf, reaching 525 °C by 30 at.% Hf addition at the expense of Ti (Refs. 3 and 16). In slightly Ni-rich compositions, the TT decreases at a rate of 10 to 15 °C per 0.1 at.% Ni (Ref. 17). However, the TT decrease can be compensated through appropriate post heat treatments (Refs. 18 to 20). Although the ternary element addition, such as Hf, is known to increase the TT when compared to NiTi, the Ti-rich version adversely affects some other features and results in relatively low ductility, low strength, large temperature hysteresis (>50 °C), low resistance to slip, and lack of cyclic stability (Ref. 16).

To date, different techniques have been used to process NiTiHf, including vacuum induction melting (VIM), vacuum arc melting (VAM), cold crucible levitation melting (CCLM), copper boat induction melting (CBIM), electron beam melting (EBM), and plasma arc melting (PAM) (Refs. 3 and 21 to 25). It is well known that the processing and machining NiTi-based alloys, including NiTiHf, is a difficult task due to the high reactivity of the alloy, stress-induced martensite, spring back effects, work hardening, burr formation, and adhesion (Refs. 26 to 29). These altogether have limited the geometry of NiTiHf components to sheets, strips, wires, tubes, or bars. Additive manufacturing (AM) techniques open up possibilities to circumvent challenges in conventional manufacturing (Refs. 28, 30, and 31). In AM techniques, the final component is being fabricated from a virtually sliced computer-aided design (CAD) model, which enables the production of complex geometries (e.g., lattice-like, truss-based, curved holes, engineered porosity, and hollow parts) (Refs. 32 and 33). Despite its high potential, no work has been performed on the AM of NiTiHf in literature. To successfully fabricate a new material (i.e., NiTiHf), the processing parameters (e.g., scanning velocity, laser power and focusing, hatch spacing, and layer thickness) must be optimized. It is worth noting that the thermomechanical features of NiTiHf add to the complexity of fabrication. In this paper, a Ti-rich NiTiHf alloy was processed for the first time via selective laser melting (SLM), the most common AM technique for powder metals. In addition, the mechanical and thermomechanical features of SLM NiTiHf compared to conventionally processed alloys were investigated.

Materials and Procedures

A slightly Ti-rich $Ni_{49.8}Ti_{30.2}Hf_{20}$ (at.% of measured composition) alloy was produced by the vacuum induction skull melting process. Part of the cast ingots were vacuum homogenized at 1050 °C for 72 h, followed by hot extrusion at 900 °C (alloy designated FS #4). Other ingots were subjected to an electrode induction-melting gas atomization (EIGA) by TLS Technik GmbH (Bitterfield-Wolfen, Germany) to

TABLE I.—SELECTIVE LASER MELTING (SLM) PROCESSING PARAMETERS USED IN FABRICATING NiTiHf COMPONENTS

Effective laser power, W	Layer thickness, μm	Scanning velocity, m/s	Hatch distance, μm
250	30	1.25	120

produce the powder. EIGA is a unique technique that produces spherical powders with extremely low impurity (e.g., O, C, ceramic impurities, and N) content. A range of 25 to 75 μm particle fractions was used to ensure a good compromise of layer resolution and flowability. The Phenix™ Systems PXM is a powder-bed based SLM machine equipped with a 300 W ytterbium fiber laser manufactured by JK Lasers. The laser beam was directly focused via galvanometric mirrors producing a beam diameter of approximately 80 μm, a beam quality of $M^2 < 1.2$, and a collimated (TEM_{00}) beam with a Gaussian profile (Refs. 34 and 35). Prior to the fabrication, CAD and Phenix™ Systems software were used to create the three-dimensional model and slice it into the requisite layers, respectively. In the PXM system, a feeding piston moves upward to provide the powder. Subsequently, a metal scraper and roller collect, deposit, and compact the powder layer on the building platform. Then, a laser selectively melts and binds the powder particles to each other. Finally, the building piston drops down with a layer thickness to accommodate the next layer. This procedure is repeated until the fabrication of the fully dense component is completed. The fabrication procedure was conducted in an Ar atmosphere, which decreased the O level to 500 ppm. Table I details the processing parameters used in this research.

Chemical compositions of the as-extruded, powder, and SLM NiTiHf were quantitatively evaluated using inductively coupled plasma atomic emission spectroscopy (ICP–AES) for metallic elements and the LECO® determinators for O, N, and C content. To determine the basic microstructure of the alloys, the samples were mounted, polished, etched, and imaged in a JEOL 840 (scanning electron microscope) SEM. Differential scanning calorimetry (DSC) analyses were conducted using a TA Instruments Q1000 with a heating/cooling rate of 10 °C/min. Each specimen was cycled 10 times between 0 to 370 °C to evaluate the stability of the phase transformation temperatures. Martensite start (M_s) and martensite finish (M_f) temperatures on cooling and austenite start (A_s) and austenite finish (A_f) temperatures on heating were determined by tangent technique. Thermomechanical tests of both as-extruded and SLM-fabricated samples were conducted using an MTS® 810 servohydraulic load frame equipped with an Ameritherm Nova Star 7-kW induction heating system. A Eurotherm controller was used to control the test temperature with type K thermocouples that were spot welded directly to the middle of the sample gauge length. A heating rate of 20 °C/min was used and cooling was partially controlled. Strains were measured from the displacement of the platen surfaces using a Micro-Epsilon™ optoCONTROL 2600, noncontacting light-emitting diode (LED) based micrometer. Constant-force thermal cycling was performed in compression at stresses ranging from 0 to 500 MPa. One SLM rectangular cube component with dimensions of 2 by 2 by 5 mm, fabricated in the horizontal direction, was tested under a minimum stress of 30 MPa due to the small sample size. The extruded rods, 10 mm long by 5 mm in diameter, were tested starting at 0 MPa. Then, each sample was cycled between 50 to 450 °C at a rate of 20 °C/min in 100 MPa increments from the lowest stress to 500 MPa. Finally, each sample was tested at 0 MPa to investigate its two-way shape memory.

Results and Discussion

Table II shows the ICP results comparing the compositions of powder, as-extruded, and SLM NiTiHf. When compared to as-extruded material, the levels of Ni-loss are reported to be 0.03 at.% for the powder and 0.21 at.% for SLM material. It can be inferred that the SLM process has more influence on the Ni content than the powder preparation procedure. Ni loss associated with SLM can mostly be attributed to the fact that the Ni element tended to evaporate sooner than the other two elements during the high-power laser melting procedure (Ref. 32). The C, N, and O levels were also measured. In general, the presence of O and C contamination has been proven to stabilize precipitates such as the $Ti_4Ni_2O_x$ phase

TABLE II.—INDUCTIVELY COUPLED PLASMA (ICP) VALUES OBTAINED FOR AS-EXTRUDED, POWDER, AND SELECTIVE LASER MELTING (SLM) NiTiHf COMPONENTS

Sample	Weight, wt%	Ni, at.%	Ti, at.%	Hf, at.%	C, wt%	N, wt%	O, wt%
FS #4 as-extruded	171.2	Reference	Reference	Reference	0.0040	0.0020	0.0433
Powder	150.9	–0.03	0.06	–0.03	0.0053 0.0054	0.0018 0.0021	0.0623 0.0626
SLM	84.3	–0.21	0.00	0.22	----------	0.0014	0.075

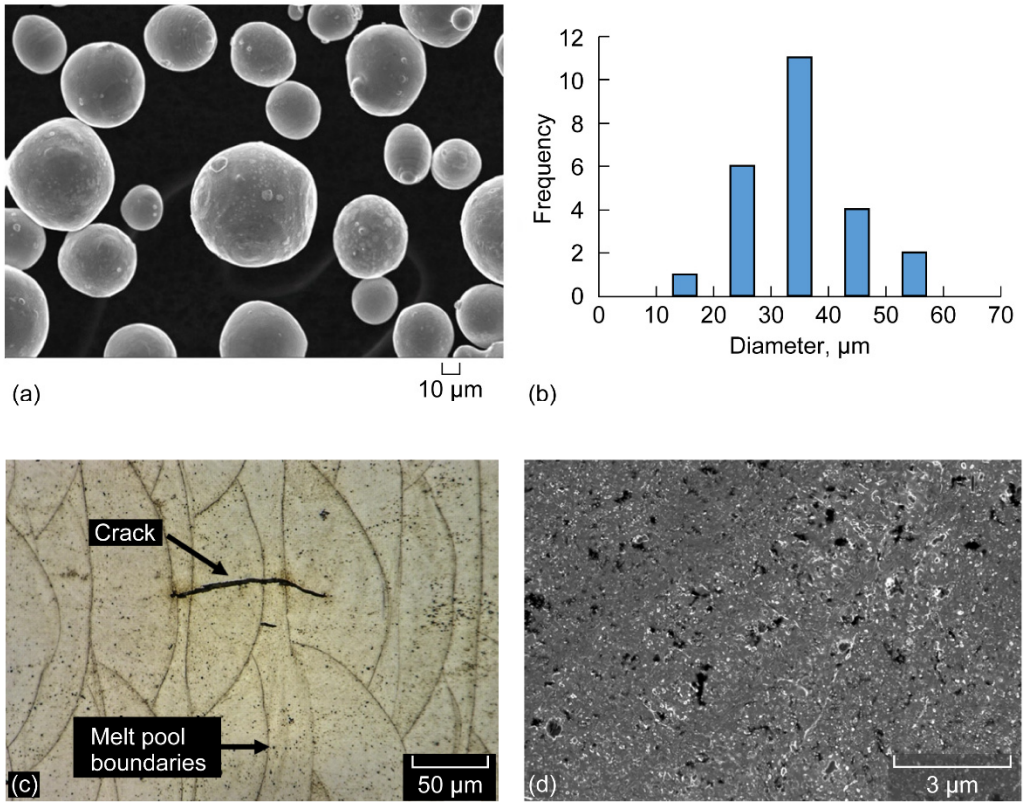

Figure 1.—Scanning electron microscopy (SEM) images. (a) Powder. (b) Particle distribution. (c) Optical. (d) Selective laser melting (SLM) NiTiHf.

(referred to Ti_2Ni-type), TiO, and TiC within the NiTi matrix (Refs. 36 to 38). According to ICP results, there is a small O gain in the powder, commonly seen in most SLM NiTi alloys, and there is additional O content introduced during the SLM process (Ref. 39). Alternatively, C gain is almost negligible during the SLM process when compared to the as-extruded alloy. Therefore, it is expected to observe $Ti_4Ni_2O_x$ phase and TiO, but not TiC, precipitates in the SLM NiTiHf alloy.

The SEM image of the powder is shown in Figure 1(a) and the particle size distribution is shown in Figure 1(b). The average size of the particles measured was 35 µm. Figures 1(c) and (d) show the optical microscopy and the SEM images of the SLM NiTiHf, respectively. The optical image of SLM NiTiHf clearly displays the formed microcracks and melt pools during fabrication. The microcrack formation can be attributed to thermal stresses resulting from rapid solidification (Ref. 32). The SEM image of SLM NiTiHf illustrates that tiny pores and finely dispersed nanosized particles are presented in the SLM NiTiHf. It is expected that these pores and the associated particles (e.g., oxides and carbides) can be tuned or reduced by optimizing the laser parameters.

Figures 2 and 3 demonstrate the DSC curves of as-extruded, powder, and SLM NiTiHf. For the SLM method, the M_s, M_f, A_s, and A_f were found to be 257, 193, 273, and 331.5 °C, respectively. The DSC results show that M_s decreases after powder atomization and increases slightly after SLM. The increase in TT is mostly attributed to the preferential evaporation of Ni during SLM processing, which shifts the matrix composition to higher Ti content that typically leads to an increase in the TT (Refs. 32 and 40). The ICP results in Table II also confirm the Ni evaporation after SLM processing. When compared to the as-extruded material, the TT of the SLM material is slightly lower, although it is expected to see higher TT for SLM due to less Ni in the matrix. This observation can be explained via ICP results, where higher levels of O content were observed for the SLM NiTiHf alloy. In general, the solubility of O is almost negligible in the NiTi matrix, and therefore, the extra O results in the possible formation of the $Ti_4Ni_2O_x$ phase as well as TiO precipitates, which in turn deplete Ti (or increase Ni) in the NiTi matrix (Refs. 41 and 42). Finally, the overall increase in the Ni/Ti ratio within the NiTiHf matrix increased the TT, as have been proven by Tang et al. (Ref. 43), Khalil-Allafi et al. (Ref. 44), and Frenzel et al. (Ref. 45). Another observation is that the SLM material demonstrates broader transformation range compared to as-extruded, mostly attributed to the inclusions during the SLM procedure as shown in Figure 1(d) (Ref. 46). It should be noted that the samples are not homogenized after SLM fabrication, however.

Figure 3 also evaluates the thermal stability, which is essential for most NiTiHf applications (Ref. 16). All three alloys exhibit good thermal stability, showing a degradation of TT for the first cycle, after which the TT remains approximately constant. The high TT decrease after the first cycle is mostly attributed to the so-called “stabilization effect,” which vanishes after the first cycle.

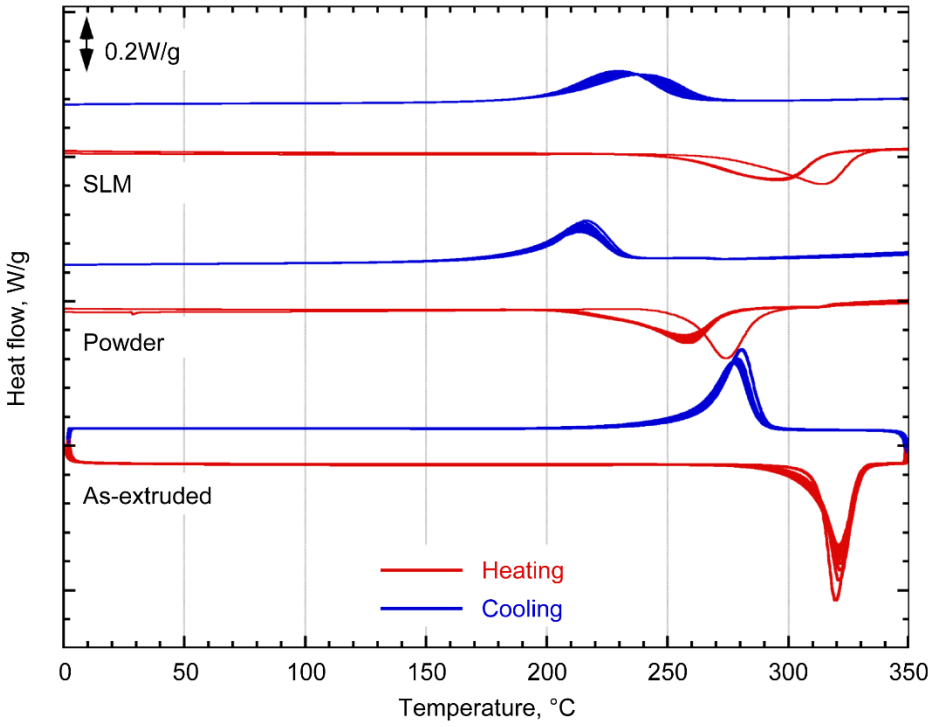

Figure 2.—Differential scanning calorimetry (DSC) curves for $Ni_{49.8}Ti_{30.2}Hf_{20}$ for selective laser melting (SLM), powder, and as-extruded NiTiHf.

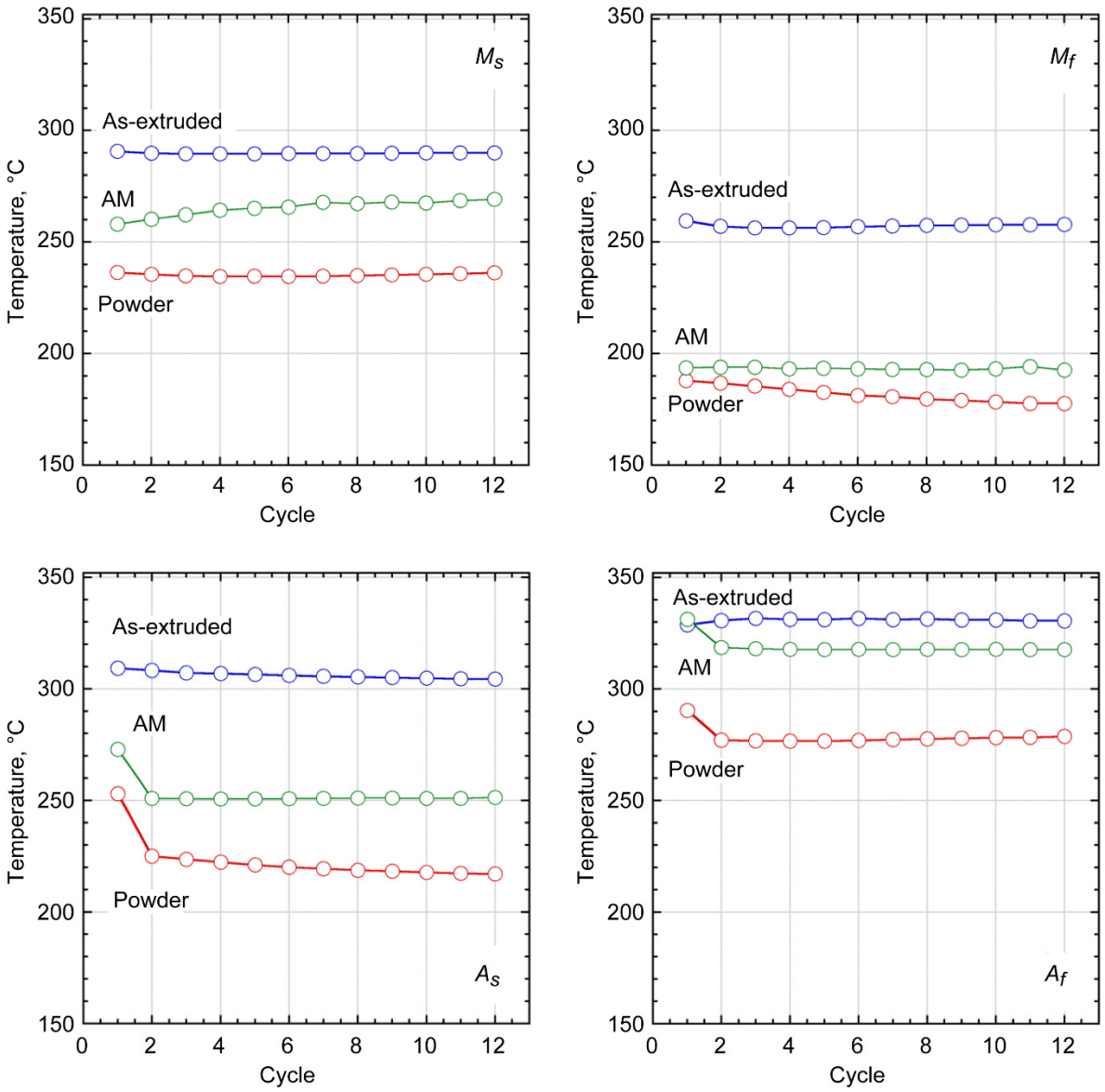

Figure 3.—Differential scanning calorimetry (DSC) curves for $Ni_{49.8}Ti_{30.2}Hf_{20}$ as a function of cycle number.

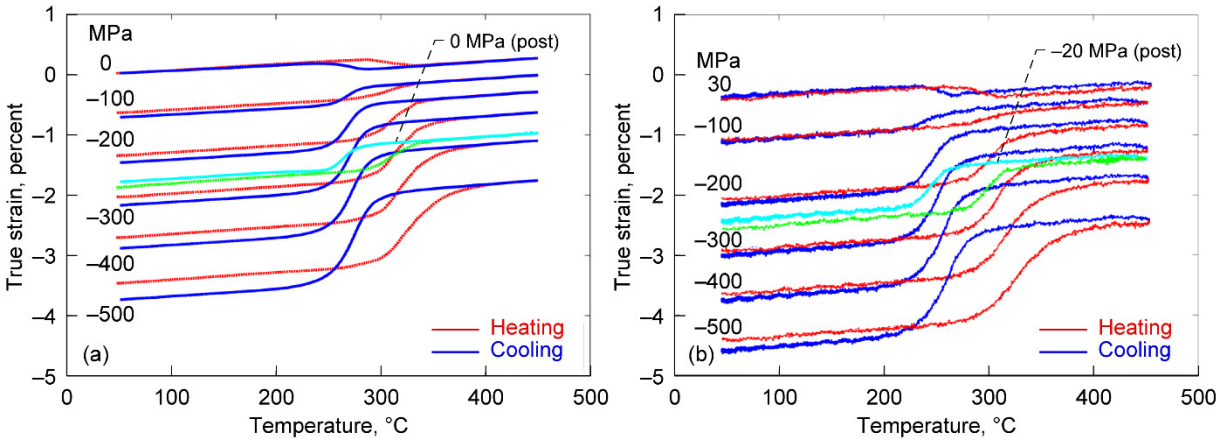

Figure 4.—Constant-force thermal cycling of the $Ni_{49.8}Ti_{30.2}Hf_{20}$ alloy under compression: (a) as-extruded and (b) selective laser melting (SLM). The red and blue curves indicate heating and cooling cycles, respectively.

Figure 4 demonstrates the constant-force thermal cycling response of $Ni_{49.8}Ti_{30.2}Hf_{20}$ under applied constant compressive stress levels, and the corresponding stress-free thermal cycling responses tested after the experiments for as-extruded and SLM components to evaluate the two-way shape-memory effect (TWSME). From a broad perspective, both the as-extruded and SLM NiTiHf demonstrate similar thermomechanical responses under the imposed stress. It is shown the SLM material exhibited larger hysteresis, in agreement with the DSC data of Figures 2 and 3. It is expected that this behavior results from the as-fabricated parts and can be improved after solution heat treatment as shown in other NiTi-based systems. Moreover, comparing the stress-free response before and after the experiments, the shape memory response is improved for both as-extruded and SLM samples, which is indicative of two-way shape memory response, although exhibiting small magnitudes (labeled “post” in Fig. 4). It is worth noting that in cases where the two-way shape memory properties are desirable, appropriate training procedures are required.

Figure 5(a) demonstrates a summary of the transformation temperatures obtained in each cycle under selected stress levels up to 500 MPa for both as-extruded and SLM NiTiHf alloys. In almost all cases, the TT attributed to as-extruded is higher than the SLM alloy. Again, this observation can be explained by the fact that the SLM alloy contains higher level of O, and therefore, a higher amount of TiO and/or $Ti_4Ni_2O_x$ phases, leading to lower TTs (Refs. 25 and 45). In general, TT increased with applied stress. Further, thermal hysteresis, measured as $A_f - M_s$, increased from 43.7 to 61.7 °C for as-extruded and from 45.6 to 80.6 °C for SLM material with increased stress. Figure 5(b) demonstrates transformation strain at each cycle for both as-extruded and SLM NiTiHf alloys. At elevated levels of stress (100 to 500 MPa), a greater net shape change is observed for SLM material compared to as-extruded. The transformation strain increased from 0.24 to 1.26 percent for the as-extruded and from 0.24 to 1.52 percent for SLM when the applied stress was increased from 100 to 500 MPa, respectively. Higher stress levels are able to reorient more of the martensite twins in an orientation that favors the applied strain during reverse transformation, which results in the availability of more strain to be recovered during the forward transformation. In general, each alloy has a critical point where this reorientation effect is maximized, however, the existence of high internal and external stresses does not allow for full recovery. Therefore, starting from the critical point, the transformation strains begin to decrease (Ref. 38). It is clear that the critical point is not in the range of selected applied stress for this study. Finally, Figure 5(c) demonstrates that the irrecoverable strain increases with higher level of applied stress for both cases. It can be observed that the irrecoverable strains of the two materials are essentially identical.

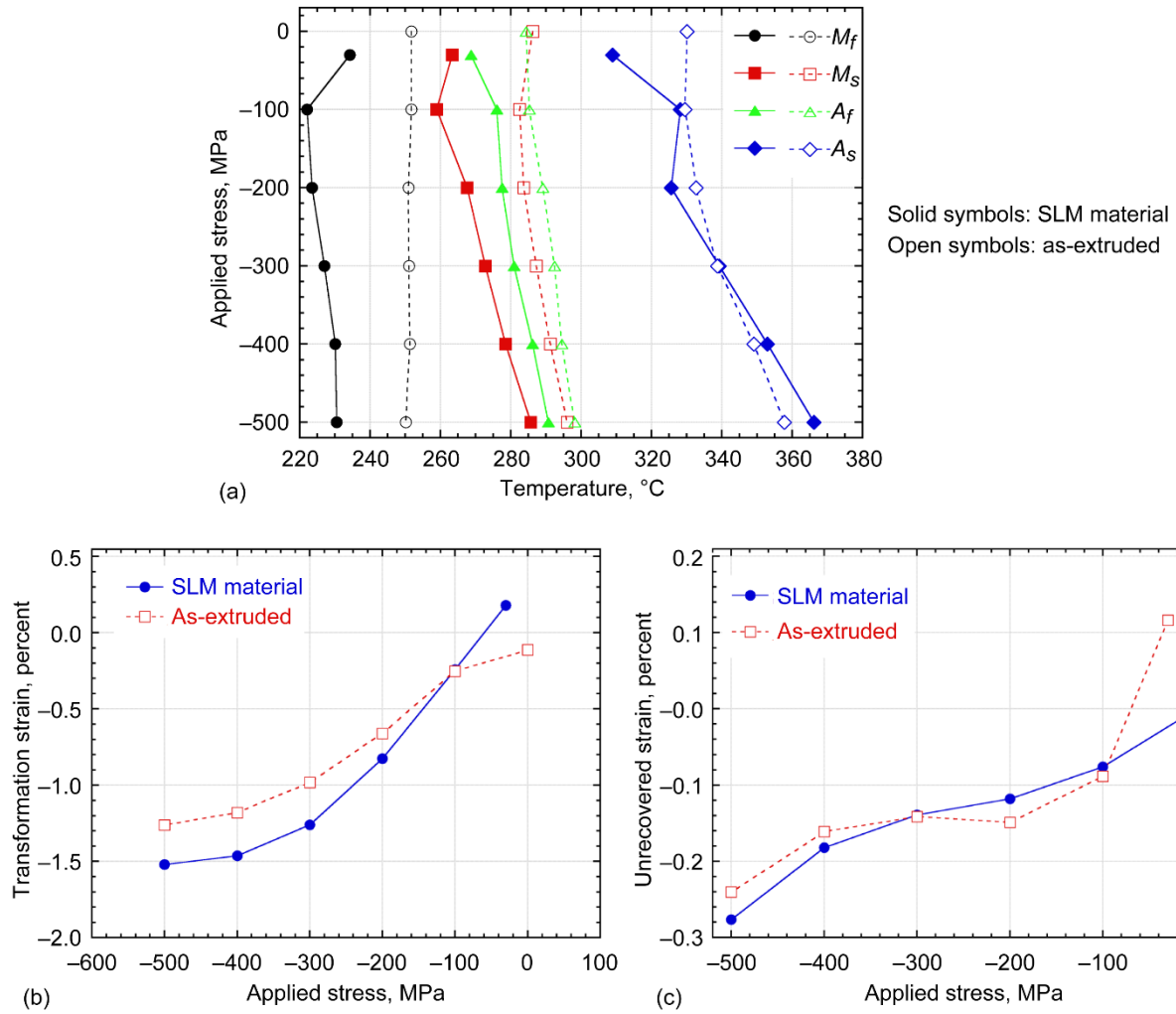

Figure 5.—Transformation characteristics: (a) transformation temperatures, (b) transformation strain, and (c) unrecoverable strain vs. applied stress of $Ni_{49.8}Ti_{30.2}Hf_{20}$ in the as-extruded (dotted lines) and selective laser melting (SLM) (solid lines) samples.

Conclusions

In summary, by using a selective laser melting (SLM) system (PXM) by Phenix™/3D Systems, NiTiHf rectangular cubes were directly manufactured using powder material. Subsequently, the thermal and functional properties of SLM NiTiHf components were evaluated via DSC and thermomechanical testing and then compared to as-extruded NiTiHf. Composition analysis shows Ni loss and O gain after SLM processing due to the associated high-power laser melting. Finely dispersed particles, pores, and cracks were observed after SLM. Thermal analysis demonstrates that the TT is slightly shifted to lower values after SLM processing, compared to the as-extruded material. This is likely attributed to the formation of secondary Ti-rich phases during atomization and the SLM technique. The microstructural analysis confirms the existence of Ti-rich secondary phases. The constant-force thermal cycling response of the SLM material demonstrated higher transformation strains, but identical trend, with as-extruded material. Finally, the stress-free thermal cycling responses of both SLM and as-extruded material exhibited small magnitudes of two-way shape memory. The microstructure and laser optimization will be a subject of future studies. Furthermore, before transition into more complex shapes, this material will be further evaluated and examined in tension and/or torsion to determine the effect of inclusions and cracks on the functional response and durability.

References

1. Hartl, Darren J.; Chatzigeorgiou, George; and Lagoudas, Dimitris C.: Three-Dimensional Modeling and Numerical Analysis of Rate-Dependent Irrecoverable Deformation in Shape Memory Alloys. Int. J. Plasticity, vol. 26, no. 10, 2010, pp. 1485–1507.
2. Hsu, D.H. Dai, et al.: The Effect of Aluminum Additions on the Thermal, Microstructural, and Mechanical Behavior of NiTiHf Shape Memory Alloys. J. Alloys Compd., vol. 638, 2015, pp. 67–76.
3. Kockar, B., et al.: A Method To Enhance Cyclic Reversibility of NiTiHf High Temperature Shape Memory Alloys. Scripta Mater., vol. 54, 2006, pp. 2203–2208.
4. Bucsek, Ashley N., et al.: Composition, Compatibility, and the Functional Performances of Ternary NiTix High-Temperature Shape Memory Alloys. Shap. Mem. Superelasticity, vol. 2, 2016, pp. 62–79.
5. Firstov, G.S.; Van Humbeeck, J.; and Koval, Yu.N.: Comparison of High Temperature Shape Memory Behaviour for ZrCu-Based, Ti–Ni–Zr and Ti–Ni–Hf Alloys. Scripta Mater., vol. 50, 2004, pp. 243–248.
6. Evirgen, A., et al.: Role of Nano-Precipitation on the Microstructure and Shape Memory Characteristics of a New Ni50.3Ti34.7Zr15 Shape Memory Alloy. Mater. Sci. Eng. A, vol. 655, 2016, pp. 193–203.
7. Mohanchandra, K.P.; Shin, Daniel; and Carman, G.P.: Deposition and Characterization of Ti-Ni-Pd and Ti-Ni-Pt Shape Memory Alloy Thin Films. Smart Mater. Struct., vol. 14, 2005, pp. S312–S316.
8. Casalena, L., et al.: Transformation and Deformation Characterization of NiTiHf and NiTiAu High Temperature Shape Memory Alloys. Microsc. Microanal., vol. 21, 2015, pp. 607–608.
9. Casalena, Lee, et al.: Mechanical Behavior and Microstructural Analysis of NiTi-40Au Shape Memory Alloys Exhibiting Work Output Above 400 °C. Intermetallics, vol. 86, 2017, pp. 33–44.
10. Benafan, O., et al.: In Situ Neutron Diffraction Study of NiTi-21Pt High-Temperature Shape Memory Alloys. Shap. Mem. Superelasticity, vol. 2, 2016, pp. 337–346.
11. Karaca, H.E., et al.: NiTiHf-Based Shape Memory Alloys. Mater. Sci. Technol., vol. 30, no. 13, 2014, pp. 1530–1544.
12. Ma, J.; Karaman, I.; and Noebe, R.D.: High Temperature Shape Memory Alloys. Int. Mater. Rev., vol. 55, no. 5, 2010, pp. 257–315.
13. Benafan, O., et al.: Mechanical and Functional Behavior of a Ni-Rich Ni50.3Ti29.7Hf20 High Temperature Shape Memory Alloy. Intermetallics, vol. 50, 2014, pp. 94–107.
14. Meng, X.L., et al.: Effect of Aging on Martensitic Transformation and Microstructure in Ni-Rich TiNiHf Shape Memory Alloy. Scripta Mater., vol. 54, 2006, pp. 1599–1604.
15. Saghaian, S.M., et al.: Effects of Ni Content on the Shape Memory Properties and Microstructure of Ni-Rich NiTi-20Hf Alloys. Smart Mater. Struct., vol. 25, 2016, p. 095029.
16. Karaca, H.E., et al.: Effects of Nanoprecipitation on the Shape Memory and Material Properties of an Ni-rich NiTiHf High Temperature Shape Memory Alloy. Acta Mater., vol. 61, 2013, pp. 7422−7431.
17. Angst, D.R.; Thoma, P.E.; and Kao, M.: The Effect of Hafnium Content on the Transformation Temperatures of Ni49Ti51−xHfx. Shape Memory Alloys, J. Phys. IV France, vol. 5, 1995, C8−747—C8−752.
18. Meng, X.L., et al.: Shape-Memory Behaviors in an Aged Ni-Rich TiNiHf High Temperature Shape-Memory Alloy. Intermetallics, vol. 16, no. 5, 2008, pp. 698−705.
19. Saedi, Soheil, et al.: Texture, Aging, and Superelasticity of Selective Laser Melting Fabricated Ni-Rich NiTi Alloys. Mater. Sci. Eng. A, vol. 686, 2017, pp. 1−10.
20. Saghaian, S.M., et al.: Effects of Aging on the Shape Memory Behavior of Ni-Rich Ni50.3Ti29.7Hf20 Single Crystals. Acta Mater., vol. 87, 2015, pp. 128−141.
21. Moshref-Javadi, Mahdi, et al.: Fabrication of (Ti,Hf)-Rich NiTiHf Alloy Using Graphitic Mold and Crucible. J. Mater. Sci. Technol., vol. 30, no. 3, 2014, pp. 280−284.
22. Besseghini, S.; Villa, E.; and Tuissi, A.: Ni-Ti-Hf Shape Memory Alloy: Effect of Aging and Thermal Cycling. Mater. Sci. Technol., vol. A273−275, 1999, pp. 390−394.
23. Matsugi, Kazuhiro, et al.: Property-Control of TiNi System Intermetallics and Their Characteristics. Mater. Trans., vol. 52, no. 12, 2011, pp. 2189−2196.

24. Morita, Arimichi, et al.: Alloying Titanium and Tantalum by Cold Crucible Levitation Melting (CCLM) Furnace. Mater. Sci. Eng. A, vol. 280, 2000, pp. 208−213.
25. Bigelow, G.S., et al.: Load-Biased Shape-Memory and Superelastic Properties of a Precipitation Strengthened High-Temperature Ni50.3Ti29.7Hf20 Alloy. Scripta Mater., vol. 64, no. 8, 2011, pp. 725−728.
26. Biermann, D., et al.: A Study on Micro-Machining Technology for the Machining of NiTi: Five-Axis Micro-Milling and Micro Deep-Hole Drilling. J. Mater. Eng. Perform., vol. 20, no. 4, 2011, pp. 745−751.
27. Wu, M.H.: Fabrication of Nitinol Materials and Components. Mater. Sci. Forum, vols. 394−395, 2002, pp. 285−292.
28. Moghaddam, Narges Shayesteh, et al.: Metals for Bone Implants: Safety, Design, and Efficacy. Biomanuf. Rev., vol. 1, 2016.
29. Kaynak, Y., et al.: The Effects of Machining on the Microstructure and Transformation Behavior of NiTi Alloy. Scripta Mater., vol. 74, 2014, pp. 60−63.
30. Andani, Mohsen Taheri, et al.: Metals for Bone Implants. Part 1. Powder Metallurgy and Implant Rendering. Acta Biomater., vol. 10, no. 10, 2014, pp. 4058−4070.
31. Guo, Nannan; and Leu, Ming C.: Additive Manufacturing: Technology, Applications and Research Needs. Frontiers of Mechanical Engineering, vol. 8, no. 3, 2013, pp. 215−243.
32. Elahinia, Mohammad, et al.: Fabrication of NiTi Through Additive Manufacturing: A Review. Prog. Mater Sci., vol. 83, 2016, pp. 630−663.
33. Vandenbroucke, Ben; and Kruth, Jean-Pierre: Selective Laser Melting of Biocompatible Metals for Rapid Manufacturing of Medical Parts. Rapid Prototyping J., vol. 13, no. 4, 2007, pp. 196−203.
34. Kuznetsov, M., et al.: Design and Characteristics of High-Power (>0.5-W CW) Diode-Pumped Vertical-External-Cavity Surface-Emitting Semiconductor Lasers With Circular TEM/Sub 00/Beams. IEEE J. Sel. Topics Quantum Electron., vol. 5, 1999, pp. 561−573.
35. Moghaddam, N.S., et al.: Modeling of Graphene Nano-Ribbon Schottky Diodes in the Parabolic Band Structure Limit. AIP Conf. Proc., vol. 1499, no. 1, 2012, pp. 268−271.
36. Nevitt, M.V.: Stabilization of Certain Ti_2Ni-Type Phases By Oxygen. Trans. Met. Soc. AIME, vol. 218, 1960.
37. Nishida, M.; Wayman, C.M.; and Honma, T.: Precipitation Processes in Near-Equiatomic TiNi Shape Memory Alloys. Metall. Trans. A, vol. 17, no. 9, 1986, pp. 1505−1515.
38. Bigelow, Glen S., et al.: Correlation Between Mechanical Behavior and Actuator-Type Performance of Ni-Ti-Pd High-Temperature Shape Memory Alloys. Proc. SPIE 6526, 2007, p. 65262B.
39. Habijan, T., et al.: The Biocompatibility of Dense and Porous Nickel-Titanium Produced by Selective Laser Melting. Mater. Sci. Eng. C, vol. 33, 2013, pp. 419−426.
40. Halani, Pratik R., et al.: Phase Transformation Characteristics and Mechanical Characterization of Nitinol Synthesized by Laser Direct Deposition. Mater. Sci. Eng. A, vol. 559, 2013, pp. 836−843.
41. Kwarciak, J.; Lekston, Z.; and Morawiec, H.: Effect of Thermal Cycling and Ti_2Ni Precipitation on the Stability of the Ni-Ti Alloys. J. Mater. Sci., vol. 22, no. 7, 1987, pp. 2341−2345.
42. Zhang, Zhonghua, et al.: Vacuum Induction Melting of Ternary NiTiX (X= Cu, Fe, Hf, Zr) Shape Memory Alloys Using Graphite Crucibles. Mater. Trans., vol. 47, no. 3, 2006, pp. 661−669.
43. Tang, W., et al.: New Modelling of the B2 Phase and Its Associated Martensitic Transformation in the Ti-Ni System. Acta Mater., vol. 47, 1999, pp. 3457−3468.
44. Khalil-Allafi, Jafar; Dlouhy, Antonin; and Eggeler, Gunther: Ni4Ti3-Precipitation During Aging of NiTi Shape Memory Alloys and Its Influence on Martensitic Phase Transformations. Acta Mater., vol. 50, 2002, pp. 4255−4274.
45. Frenzel, J., et al.: Influence of Ni on Martensitic Phase Transformations in NiTi Shape Memory Alloys. Acta Mater., vol. 58, 2010, pp. 3444−3458.
46. Speirs, M., et al.: Fatigue Behaviour of NiTi Shape Memory Alloy Scaffolds Produced by SLM, a Unit Cell Design Comparison. J. Mech. Behav. Biomed., vol. 70, 2017, pp. 53−59.